Journal Pre-proof

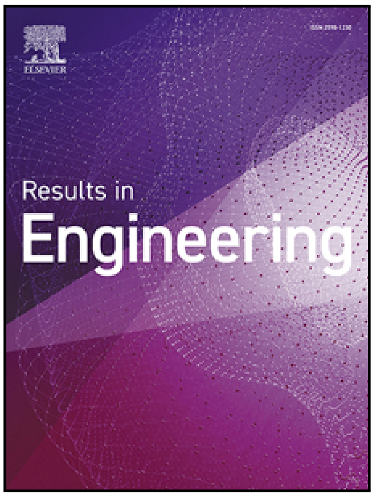

Optimizing Energy Storage and Return of Prosthetic Feet: A Biomechanical Approach Using Advanced Optimization Techniques

Aphiwat Saemua , Supakit Rooppakhun

PII: S2590-1230(25)01291-5
DOI: https://doi.org/10.1016/j.rineng.2025.105219
Reference: RINENG 105219

To appear in: *Results in Engineering*

Received date: 26 December 2024
Revised date: 12 April 2025
Accepted date: 5 May 2025

Please cite this article as: Aphiwat Saemua , Supakit Rooppakhun , Optimizing Energy Storage and Return of Prosthetic Feet: A Biomechanical Approach Using Advanced Optimization Techniques, *Results in Engineering* (2025), doi: https://doi.org/10.1016/j.rineng.2025.105219

Highlights

- A novel design framework that leverages advanced optimization techniques, including Latin Hypercube Sampling (LHS), Kriging, and Muti-Objective Genetic Algorithm (MOGA) to improve the prosthetic foot design.

- The prosthetic foot's middle and lower blade thickness are critical parameters affecting force reaction and stress distribution to minimize weight while maximizing stiffness and energy return.

- Finite Element Analysis (FEA) validated the ability of the design to withstand daily stress according to ISO 1328 standards for prosthetic testing.

Optimizing Energy Storage and Return of Prosthetic Feet: A Biomechanical Approach Using Advanced Optimization Techniques

Aphiwat Saemua and Supakit Rooppakhun*

School of Mechanical Engineering, Institute of Engineering, Suranaree University of Technology, Muang, Nakhon Ratchasima 30000, Thailand 111 University Avenue, Muang, Nakhon Ratchasima 30000, Thailand

*Corresponding Author:

Supakit Rooppakhun, Ph.D.

School of Mechanical Engineering, Institute of Engineering

Suranaree University of Technology

111 University Avenue, Suranaree Sub-District,

Muang Nakhon Ratchasima District,

Nakhon Ratchasima, 30000, Thailand

Tel: +66-4422-4252

Fax: +66-4422-4613

Email: supakit@sut.ac.th

Optimizing Energy Storage and Return Prosthetic Feet: A Biomechanical Approach Using Advanced Optimization Techniques

Abstract

Energy Storage and Return (ESR) prosthetic feet are vital in restoring natural gait biomechanics for individuals with lower-limb amputations. This study introduces a novel design framework that combines Latin Hypercube Sampling (LHS), Kriging, and a Multi-Objective Genetic Algorithm (MOGA) to optimize weight, stiffness, and energy return. Aluminum alloy was selected for its balance of strength, affordability, and manufacturability. Finite Element Analysis (FEA) validated the structural performance under ISO 10328 loading conditions. The results demonstrate that, despite aluminum having lower impact resistance than carbon fiber, its energy return during walking is comparable, differing by 19% while maintaining an appropriate Range of Motion. These findings highlight the potential of aluminum as a cost-effective alternative without compromising key biomechanical performance. The proposed framework enables the development of lightweight, resilient prosthetic feet that align with user biomechanics and may reduce overall cost barriers to solutions.

Keywords: Energy Storage and Return (ESR), Prosthetic Foot, Optimization Techniques, Latin Hypercube Sampling (LHS), Multi-Objective Genetic Algorithm (MOGA), Finite Element Analysis (FEA).

1. Introduction

Losing a leg significantly impacts an individual quality of life. Prosthetic feet are vital in restoring mobility, enabling engagement in daily activities, and improving overall well-being. Energy Storage and Return (ESR) prosthetic feet are widely used passive devices made from elastic materials, functioning like springs to store and release energy during the gait cycle [1]. The development of ESR prosthetic feet represents a major advancement in prosthetic technology, as they address the need for devices that mimic the natural biomechanics of the human foot. Optimizing the stiffness of ESR prosthetic feet is crucial for improving biomechanical performance and enhancing the functionality of individuals with lower-limb amputations.

Key factors influencing the design of ESR prosthetic feet include weight, ground reaction force (GRF), stiffness characteristics, and material selection. Lighter prosthetic feet reduce mechanical load, improving maneuverability and reducing fatigue. At the same time, heavier devices may increase strain and contribute to long-term complications [2–4]. Proper stiffness management is essential for controlling GRF, helping natural movement, and reducing the risk of musculoskeletal issues [5]. Adjusting stiffness impacts shock absorption, stability, and energy return. Lower stiffness can enhance energy return and increase the range of motion. However, it may compromise mechanical efficiency and durability, increasing the risk of damage to the prosthetic foot [6, 7]. Material selection also significantly influences prosthetic foot performance, influencing weight, stiffness, and strength. While carbon fiber and titanium offer strength and durability, their high-cost limits accessibility. Aluminum provides a lightweight, cost-effective alternative with good performance and structural integrity [8, 9]. Balancing performance, strength, and affordability is essential to ensure accessibility, as these factors directly affect user experience and their ability to engage in daily activities. Consequently, optimizing these design factors is critical for developing ESR prosthetic feet that improve performance, comfort, and overall user satisfaction.

ISO 10328 provides standardized guidelines to ensure the safety and performance of prosthetic devices by evaluating their mechanical properties and structural integrity. Several studies have focused on applying Finite Element Analysis (FEA) to evaluate ESR prosthetic feet according to these standards. Bonnet et al. [10] combined gait analysis data with FEA to model prosthetic feet stress distribution and energy storage capabilities during the stance phase, providing valuable insights for enhancing their dynamic performance. Milan Omasta et al. [11] analyzed stress distribution in the Sure-flex™ prosthetic foot, demonstrating that FEA offers detailed insights into the structural foot behavior and stress distribution under various loading conditions. Mahmoodi et al. [12] and Tryggvason et al. [13] used FEA simulations in prosthetic foot design. Mahmoodi et al. focused on optimizing the design based on rollover shape and GRF characteristics. At the same time, Tryggvason et al. investigated how material properties, such as aluminum alloys, impact structural integrity and performance. Additionally, research comparing stress levels across various materials, including aluminum alloys, titanium alloys, carbon fiber epoxy, and composite materials, has demonstrated the effectiveness of FEA in optimizing prosthetic leg design, particularly for assessing load-bearing capacities and material performance [14]. Tryggvason et al. [15] conducted dynamic simulations to predict prosthetic foot responses to design modifications, further validating the effectiveness of FEA through mechanical testing and optimization. Tabucol et al. [16] developed an ESR prosthetic foot incorporating elastic elements for energy storage and release, using FEA and optimization techniques to refine its stiffness properties and enhance functionality. Their methodology emphasizes dynamic simulations and static testing to validate performance, demonstrating the critical role of FEA in optimizing ESR prosthetic foot design.

While significant progress has been made, much of the existing research has primarily employed single-objective optimization methods or focused on high-cost composite materials, such as carbon fiber. These approaches often lack scalability and may not fully incorporate biomechanically relevant performance indicators like GRF, stiffness response, or range of motion. Additionally, few studies have investigated ESR prosthetic foot optimization using cost-effective materials like aluminum, which could improve accessibility without compromising performance. Prior work has also largely overlooked advanced metaheuristic strategies such as Multi-Objective Genetic Algorithms (MOGA) in combination with efficient sampling and modeling techniques. To address these limitations, it can be seen that the application of optimization combined with FEMS improves the results [17, 18]. This study introduces a multi-objective optimization framework for ESR prosthetic feet made from low-cost aluminum alloy. In contrast to prior studies, which often focus on a single optimization goal or high-performance composites, the present research leverages advanced techniques of Latin Hypercube Sampling (LHS) for comprehensive design space exploration, Kriging-based response surface modeling for performance estimation, and MOGA to identify Pareto-optimal designs balancing GRF, weight, and stiffness [19, 20]. This integrative approach allows for a more robust, efficient, and scalable solution.

In this study, the primary objective is to optimize the design of ESR prosthetic feet by reducing weight and increasing stiffness while maintaining an ideal GRF. This was achieved by applying advanced multi-objective optimization techniques integrated with biomechanically relevant performance indicators. Additionally, the study explores using aluminum alloy as a cost-effective alternative to high-cost composite materials, ensuring both functional performance and manufacturability.

2. Specifications

Prosthetic feet must have a robust structure supporting the weight of the amputee and facilitating daily activities. The prosthetic weight should match the residual limb to ensure proper balance and ease of movement. Additionally, the foot must withstand the forces and torque encountered during plantar flexion, providing stability and support throughout the gait cycle without reliance on external power sources. It should also exhibit resistance to impacts, ensuring durability and comfort while maintaining lateral flexibility in the frontal plane to enhance terrain adaptability [21].

Stiffness and weight influence load-bearing capacity and energy efficiency during movement. Stiffness is defined as the ratio of load to deformation, where deformation refers to the rotation of the foot in the sagittal plane, and load represents the Ground Reaction Force (GRF). During walking, ankle rotation typically ranges from −6° to −12° during initial plantar flexion and from 6° to 16° during maximum dorsiflexion prior to heel-off [22–25].

A comprehensive understanding of Ground Reaction Force (GRF) is essential for managing shock absorption, energy return, and load distribution during walking, which is critical for reducing the risk of injury. GRF generally follows a double-peaked pattern during the gait cycle: the first peak (95-120% of body weight) occurs shortly after the heel strike, and the second peak (110-135% of body weight) appears during push-off [26, 27]

3. Efficient Global Optimization (EGO)

The Efficient Global Optimization (EGO) process begins with the generation of an initial sampling of input variables using methods such as full factorial design, Central Composite Design (CCD), or Latin Hypercube Sampling (LHS) through the design of experiment (DOE). Then, inputs will be analyzed with analytical, numerical, or experimental methods to collect output data. The input-output dataset creates a surrogate model employing techniques like response surface, the Kriging method, or the Radial Basis Function (RBF) [28]. Finally, the surrogate model integrates into the Expected Improvement (EI) equation. Instead of single-objective optimization methods, multi-objective genetic algorithms (MOGA) maximize the EI equation. MOGAs use evolutionary mechanisms to identify areas of uncertainty called sampling points in the objective space. These points gather output data later, updating the surrogate model iteratively until convergence. Furthermore, the result does not give a single solution but a set of optimal solutions along the Pareto front, offering insights into trade-offs between conflicting objectives.

- *Kriging Method*

The Kriging method is a spatial interpolation technique that originated in mining geology. It uses a limited set of sample data points to estimate the value of a variable over a continuous spatial field. This powerful method predicts unknown functions by combining a global model, which captures the overall trend of the data, with a correction term that accounts for local deviations [29]. The following equation expresses the Kriging model:

$$\hat{y}(x) = \mu(x) - r^T R^{-1}(F - \mu) \tag{1}$$

Where $\mu(x)$ is the global model, and $r^T R^{-1}(F - \mu)$ is the local deviation. The global model is a constant value across the field, calculated using the following equation:

$$\mu = \frac{1^T R^{-1} F}{1^T R^{-1} 1} \tag{2}$$

The sample points x are interpolated using a Gaussian random function, with the local deviation determined by the correlation between $Z(x_i)$ and $Z(x_j)$ .This correlation depends on the distance between the respective points x_i andx_j, calculated using the Distance Function, expressed as:

$$d(x_i, x_j) = \sum_{k=1}^{m} \theta^k \left|x_i^k - x_j^k\right|^2 \tag{3}$$

Where θ^k $(0 \leq \theta^k \leq \infty)$ is the element of the correlation vector parameter,θ. The correlation between $Z(x_i)$ and $Z(x_j)$, which depends on the distance function, is expressed as:

$$\mathrm{Corr}\left[Z(x_i), Z(x_j)\right] = \exp(-d(x_i, x_j)) \tag{4}$$

- *Genetic algorithms*

Genetic algorithms (GAs) are heuristic optimization techniques of a metaheuristic that can be used to solve both constrained and unconstrained problems, such as single-objective optimization problems straight from the principles of natural selection by simulation of biological evolution [30]. The GAs start configuring the chromosome structure and create an initial random population, eventually trying to find the best solutions to ensure the rest of the higher ranks during comparisons. Then, the chromosomes are evaluated using objective functions to pinpoint the best chromosomes and calculate the fitness score of each chromosome [31]. The genetic operations, including selection, crossover, and mutation, generate new generations of chromosomes influenced by a fitness function. Crossover is the process of shuffling genes between parents to create the child of the next generation, and mutation is the infusion of random changes to various offspring. The GAs method is repeated until the target fitness function results that agree with the given chromosome are reached. Multi-objective genetic algorithms (MOGAs), on their part, follow the same principles as GAs but are designed to solve multi-objective optimization problems, the chromosomes being assessed based on multiple objectives. MOGAs aim to find a set of good solutions, forming a Pareto front that is a trade-off between different goals but has a variety of solutions [32].

- *Latin hypercube sampling*

Latin Hypercube Sampling (LHS) is a statistical method for sampling from multidimensional probability distributions. It works by dividing each input range of variables into intervals with equal probability and selecting one random sample from each interval, ensuring that every interval is sampled at least once. The process begins by defining input variables and their corresponding ranges, divided into intervals based on the number of desired samples. A value is randomly chosen from each interval, and these values are permuted to create unique sample sets. Compared to simple random sampling, Latin Hypercube Sampling (LHS) requires fewer samples to achieve comparable input space coverage due to its structured design. While LHS generates uniformly distributed samples within intervals, they can be adjusted to match other probability distributions using techniques like inverse transform sampling. This adaptability makes LHS a popular method in engineering design, simulations, sensitivity analysis, and optimization studies, where understanding how input variability affects system performance is essential [33].

4. The ISO 10328 Standard Static Test

The safety verification of Energy Storage and Return (ESR) prosthetic feet is commonly performed through static tests regulated by ISO 10328 standards. These tests are divided into the dorsiflexion test (toe test) and the plantar flexion test (heel test). In the toe test, a settling force is applied to the forefoot at an angle of 20 degrees. In contrast, in the heel test, the force is applied to the heel at an angle of 15 degrees, as depicted in Fig. 1. The forces are applied at a rate between 100 N/s and 250 N/s, maintained for 30 ± 3 seconds, and then removed.

For the dorsiflexion test, the settling forces applied at the forefoot are 108%, 106%, and 104% of the body weight for individuals weighing 60 kg, 80 kg, and 90 kg, respectively. For the plantar flexion test, the settling forces at the heel are 125%, 120%, and 116% of the body weight for the same weight categories [34].

5. Materials and Methods

In this study, the prosthetic foot design was inspired by the Pro-Flex Pivot by Össur. It was organized into three functional groups: the ankle structure group (pylon connector and ankle body), the connection group (link and holder), and the foot group (lower blade, middle blade, and upper blade). The initial geometry was defined based on anatomical parameters, including the foot length (L), the ankle joint height (h) from the ground, and the distance (d) from the ankle joint to the heel, approximately one-third of the foot length. For this study, the foot length was set at 250 mm, and the ankle joint height was varied between 80 mm and 100 mm, as illustrated in Fig. 2.

The design emphasizes the foot group, which comprises the elastic components responsible for energy storage and return. During the early stance phase (heel strike), loading at the heel causes a deflection in the heel portions of the lower and middle blades. In contrast, during the late stance phase (toe-off), deflection shifts to the upper and middle blades, as illustrated in Fig. 3. These deflections facilitate plantar flexion and dorsiflexion.

Geometry optimization was performed using 2D Finite Element Analysis (FEA) to refine the profiles of elastic components, enhancing the energy-storing capabilities of the Energy Storage and Return (ESR) foot. This step is crucial because Ground Reaction Force (GRF) and stiffness play a pivotal role in prosthetic foot design by influencing stability, energy efficiency, and comfort. GRF interacts with stiffness to govern the foot's resistance to deformation; excessive stiffness limits shock absorption, while insufficient stiffness increases deformation and fall risk. A balance between GRF and stiffness ensures stability, efficient energy return, and safe adaptation to varying gait dynamics.

The CAD model was constructed in the x–y plane and imported into ANSYS Workbench for 2D static structural analysis. Following ISO 10328 standards, the plantar flexion test was performed by applying load at the heel, while the dorsiflexion test involved loading at the forefoot. The 10 mm and 30 mm displacements were applied to the plantar flexion and dorsiflexion testing platforms, respectively. The shank was fixed at the pylon connector's top to ensure loading stability. The applied loads, boundary conditions, and displacements used in this analysis are illustrated in Fig. 4.

For contact modeling and realistic interactions, a no-separation contact type was applied between the pylon connector and ankle body, representing the ankle joint with frictionless motion. The contact between the ankle body and upper blade was modeled as bonded. Frictional contacts with a coefficient of 0.20 were used for the upper, middle, and lower blades to reflect material interaction under the load. According to joint modeling, the pretension bolts were modeled as preloaded springs with forces specific to each joint. The bolts connecting the blades were modeled as longitudinal spring elements. The pretension forces for M6 (7.54 kN) and M8 (13.8 kN) bolts were applied as normal forces. Links between the pylon connector and holder were modeled with body-to-body beam elements. The FEA model was developed in ANSYS Workbench using a quadrilateral dominant method and quadratic elements to ensure accurate stress and displacement analysis. In this study, mesh convergence analysis was conducted to confirm that the finite element results were independent of further mesh refinement. Element sizes between 10.0 mm and 2.0 mm were tested. Convergence was achieved when the change in equivalent stress was less than 2%, as shown in Fig. 5. The results indicated that the equivalent stress difference between the 4 mm and 2 mm mesh sizes was 0.218% with 2,812 elements for the dorsiflexion test and 0.528% with 2,686 elements for the plantar flexion test, validating the chosen mesh resolution.

Under the simulation, a 2D FEA model of the prosthetic foot was developed using nonlinear static structural analysis to capture the complex behavior of the foot's elastic components under load. While the material is assumed to be linearly elastic, the nonlinear behavior arises from significant deflections and the interactions between components under load, which were appropriately modeled. The simulation results were crucial for assessing the prosthetic foot's mechanical performance, providing valuable insights into its design. Key outputs, such as Ground Reaction Force (GRF), total volume, and Range of Motion (ROM), were analyzed to evaluate the foot's stiffness, stability, energy return, and weight. The reaction force at the fixed boundary condition directly reflects the foot stiffness, with an increased reaction force indicating higher stiffness, which enhances stability and energy return. Conversely, a lower reaction force suggests reduced stiffness, potentially compromising energy storage and return efficiency. The total volume determines the foot's weight and is a critical factor influencing comfort, stability, and mobility. A lighter foot improves comfort and reduces fatigue. A heavier foot may provide added stability but limit performance and energy return. Additionally, the elastic components of the foot group regulate ROM through deflection, enabling plantar flexion and dorsiflexion. Geometry optimization ensures that ROM remains within functional limits, preventing instability or excessive movement.

Under standard static testing conditions, stress concentrations in the prosthetic foot are primarily observed at the foot end due to deflection, marking a critical failure point. As shown in Fig 6, the design variables are initialized within specified ranges in Table 1. Latin Hypercube Sampling (LHS) generates initial sampling points, ensuring a diverse, non-repeating distribution across the vertical and horizontal axes. This method allows flexibility in determining the number of samples for optimization.

A case study of prosthetic feet was conducted and assumed to be linear elastic, homogeneous, and isotropic materials. In this study, aluminum alloy 6061-T6 was used for prosthetic feet. The mechanical properties of aluminum alloy 6061-T6, as shown in Table 2, were obtained from previous literature [35].

In the finite element simulations, the prosthetic foot was assumed to be made of linear elastic, homogeneous, and isotropic aluminum alloy (6061-T6), with material properties adopted from literature. A plane stress 2D model was used, assuming negligible out-of-plane effects. All loads were applied quasi-statically, and dynamic or inertial effects were not considered. Frictional contact was modeled between key interfaces (with a coefficient of 0.2). At the same time, fixed supports were applied at the distal bolt holes to simulate fixation during loading. These modeling assumptions are consistent with previous early-stage prosthetic foot design optimization studies.

6. Results and Discussion

- *Model Validation*

The predicted versus observed graph shown in Fig. 7 assesses the accuracy of the Kriging surrogate model in optimizing ESR prosthetic feet. It displays the correlation between predicted and observed values for key response parameters: P7 (total volume in mm³), P8 (maximum force at the toe in N), P9 (equivalent stress at the toe in MPa), P10 (maximum force at the heel in N), and P11 (equivalent stress at the heel in MPa). The lines represent each parameter, with data points close to the diagonal indicating high prediction accuracy. High R^2 values, approaching 1, validate the model ability to capture response variability, confirming its effectiveness for optimizing tasks to enhance durability and performance.

- *Sensitivity Analysis*

A sensitivity analysis was conducted to assess the influence of six key design parameters on five critical output variables, as shown in Fig. 8, including Total Volume (P7), maximum reaction force at the toe (P8), maximum equivalent stress at the toe (P9), maximum reaction force at the heel (P10), and maximum equivalent stress at the heel (P11). The results reveal that the lower blade thickness (P2) is most sensitive to total volume (P7), contributing nearly 50%. The middle blade length (P4) contributes approximately 20%. For the maximum reaction force at the toe (P8), P2 reduces the force by about 27%. P5 increases it by 24%, and P5 has a moderate influence on maximum equivalent stress at the toe (P9), contributing 10-15%. At the heel (P10), the lower blade thickness (P2) is the most influential, contributing nearly 70%, with P4 and P3 also contributing positively. For maximum equivalent stress at the heel (P11), P2 reduces the stress by about 13%, while P3 increases it by 12%. It can be seen that some parameters have a higher sensitivity to specific outputs, such as the lower blade thickness (P2) because it constitutes a substantial proportion of the prosthetic foot’s structural volume. An increase in its thickness directly affects the overall mass. It enhances stiffness, particularly under heel loading during the initial stance phase.

- *Response Surface*

Fig. 9 presents the response surface chart of the relationship between the maximum reaction force at the Toe (P8) and two critical design parameters: middle blade length (P4) and upper blade thickness (P5). The chart reveals that shorter blade lengths (P4) of approximately 155 mm and thicker upper sections P5 greater than or equal to 9 mm result in higher force reactions, peaking at approximately 1.1 kN. In contrast, longer blade lengths (P4) of approximately 170 mm and thinner upper sections (P5) of approximately 5 mm reduce force reactions, reaching about 0.65 kN. The gradient, ranging from blue (lower forces) to red (higher forces), highlights this transition. Notably, reaction forces are more sensitive to changes in P5 when P4 is shorter. For optimal performance, designs should favor longer middle blade lengths and thickness of upper blade thickness, avoiding configurations with shorter blades and thin sections, as these increase the risk of localized stress and failure.

Fig. 10 presents the response surface chart of the relationship between maximum equivalent stress at the toe (P9) and two critical parameters: middle blade length (P4) and upper blade thickness (P5). The chart shows that when the middle blade length (P4) is between 165 mm and 170 mm and the upper blade thickness (P5) ranges from 8 mm to 10 mm, the equivalent stress remains relatively low, between 210-250 MPa. These suggest that certain combinations of these design parameters mitigate stress concentrations, potentially enhancing the structural blade performance. Conversely, as P4 between 150 mm and 155 mm and P5 between 5 mm and 10 mm, the equivalent stress rises significantly, reaching up to 390 MPa. This trend emphasizes carefully optimizing these parameters to avoid excessive stress concentrations. The color gradient, from blue (low stress) to red (high stress), reinforces the sensitivity of stress levels to variations in P4 and P5. For optimal design, focusing on the regions with lower stress values is crucial, particularly within the blue-green areas (e.g., P4 between 160 mm and 165 mm and P5 between 7 mm and 8 mm). These areas offer a favorable balance between minimizing stress and maintaining structural integrity, essential for optimizing blade performance and durability.

Fig. 11 presents the response surface chart of the relationship between the maximum reaction force at the heel (P10) and the critical design parameters of middle blade thickness (P3) and lower blade thickness (P2). The chart reveals that increasing middle blade thickness (P3) results in higher reaction force, especially when lower blade thickness (P2) is also high. Conversely, lower values of P2 around 4 mm reduce force reactions, even with a high P3. The color gradient, from blue (low force reactions) to red (high force reactions), highlights the significant impact of both parameters. The steepest gradients occur when P2 and P3 approach 10 mm, indicating elevated forces at the heel and emphasizing the need for careful structural design. While reducing both parameters minimizes force reactions, it may compromise load-bearing capacity. Optimizing P2 and P3 is crucial for balancing force distribution, ensuring structural strength, and enhancing durability.

Fig. 12 presents the response surface chart of the relationship between maximum equivalent stress at the heel (P11) and two critical parameters: middle blade thickness (P3) and lower blade thickness (P2). The chart reveals those lower values of P3 around 7 mm and P2 at 4 mm and 10 mm result in lower stress, approximately 180 MPa to 210 MPa. These indicate that thinner blades reduce stress concentrations and may increase structural strength. In contrast, increasing P3 to 10 mm and P2 to 6.5 mm and 7.5 mm increases stress up to 275 MPa, highlighting the impact of thickness on stress distribution. The color gradient, from blue (low stress) to red (high stress), shows moderate increases in P2, and highly valuable P3 can significantly elevate stress. The analysis underscores the importance of balancing P3 and P2 to avoid high-stress concentration, which could affect durability.

- *Tradeoff Chart*

Fig. 13 presents the response surface chart of the relationship between the total volume (P7) and maximum reaction force at the toe (P8). This chart identifies optimal trade-offs between minimizing material usage and controlling force reactions, essential for material efficiency and structural performance. The total volume (P7) is plotted on the x-axis, ranging from 5.39×10^5 mm^3 to 6.69×10^5 mm^3, while the maximum force reaction at the toe (P8) is shown on the y-axis, varying from 600 N to 1,100 N. A color map from blue (the best Pareto front) to red (the worst Pareto front) is used, with green dots representing feasible configurations that meet design constraints. A positive correlation is observed between volume and force reaction, with smaller volumes associated with lower force reactions in the blue and cyan regions. Larger volumes, particularly those above 6.1×10^5 mm^3, lead to increased force reactions and higher stress risks. Optimal designs are found in the green and cyan areas, where volume and force reactions are balanced. In summary, the Tradeoff Chart is an essential tool for optimizing designs by balancing material volume and force reactions, focusing on configurations in the green and cyan zones to get energy return during walking and lightweight.

Response Surface Analysis (RSA) reveals key parameter interactions, providing insights into selecting optimal designs. The tradeoff chart visually represented these, illustrating the compromises between weight, force reaction, and equivalent stress. Table 3 presents the design parameters for five candidate points. In contrast, Table 4 summarizes their corresponding performance outputs, demonstrating a balance between material efficiency, durability, and biomechanical function.

This study explores the optimization of ESR prosthetic feet by integrating Kriging surrogate modeling and Multi-Objective Genetic Algorithms (MOGA). The results underscore the significance of Ground Reaction Force (GRF) in influencing biomechanical performance, including stiffness and stress distribution. These findings validate the design's energy return, structural strength, and weight reduction, aligning with prior studies while enhancing the scope of optimization techniques used. This comprehensive analysis allows for addressing multiple design objectives concurrently, which is a step forward compared to more traditional, single-objective prosthetic foot designs.

The approach employed in this study combines Latin Hypercube Sampling (LHS), Kriging surrogate modeling, and MOGA to optimize ESR prosthetic feet. The Kriging model, with a high R^2 approaching 1, confirms its accuracy in predicting key responses, as noted by Li et al. [19]. The iterative optimization process driven by MOGA effectively balances conflicting objectives such as weight and stiffness, offering a more comprehensive solution than single-objective optimization methods. A key improvement of this study is using LHS, which ensures a thorough exploration of the design space, minimizing potential biases present in earlier studies that used simplified sampling methods.

In further analysis, Table 3 outlines the design parameters used to create the prosthetic foot's shape, which directly impacts its performance evaluation, including reaction forces, weight, range of motion, and stress distribution. The design analysis confirmed that Candidate Point 5 demonstrated the highest reaction forces at the forefoot (1,367.30 N) and heel (1,901.70 N). However, it was not the optimal choice. The excessive force required to achieve the proper gait angle and energy return could increase the load on the knee joint, potentially leading to osteoarthritis. On the other hand, Candidate Point 5, with a lower force reaction at the heel (249.48 N), lacked the energy return needed for effective walking. Candidate Points 1, 2, and 3, however, showed force reactions consistent with the GRF observed in the studies by Ferris et al. [26] and

Grabowski and D'Andrea [27], supporting biomechanical harmony. Among these, Candidate Point 2 was identified as the most balanced configuration, with force reaction values of 788.89 N at the toe and 707.59 N at the heel. This configuration, weighing approximately 1.46 kg, also maintained equivalent stress values below the material's yield strength (275 MPa), representing a compromise between energy return, structural strength, and weight. These results align with previous research and emphasize the critical role of balance, stiffness, and weight in optimizing mobility and reducing user fatigue. Additionally, ankle rotation for Candidate Points 1, 2, and 3 remained within the acceptable ranges documented in the literature [22–25], further confirming their practical applicability. Candidate Point 2 exhibited a higher GRF than Candidate Point 1. At the same time, Candidate Point 3 demonstrated versatility by catering to a broader range of users with varying body weights.

A more refined assessment of prosthetic foot stiffness necessitates considering both the heel and toe loading phases separately. In the heel test, simulating the initial impact of heel strike during gait, the aluminum-based design produced a higher GRF than carbon fiber-based prosthetics. This result aligns with the material properties of aluminum, which, due to its higher modulus and lower damping capacity, absorbs less impacted energy and transmits greater force back to the user. Conversely, during the toe-off phase, reflected in the toe test, the GRF values observed in the aluminum design were comparable to those in carbon composite designs, as shown in Fig. 14. This suggests that, despite aluminum's limitations in impact absorption, it can still offer similar energy return during the propulsion phase. Furthermore, the resulting Range of Motion (ROM) remained within acceptable limits defined by existing prosthetic foot standards, ensuring functional usability. These highlight the importance of material selection in balancing cost and performance in prosthetic foot design. These findings indicate that, with appropriate optimization, aluminum can serve as a viable low-cost alternative to carbon fiber in ESR prosthetic feet, maintaining essential biomechanical characteristics. Given the relatively lower cost of aluminum alloys, this approach could facilitate broader access to high-performance prosthetic devices, especially for users in low-resource settings.

The study's findings are consistent with existing biomechanics research on prosthetics. Bonnet et al. [10] and Omasta et al. [11] used FEA to assess the stress distributions of foot prosthetics, identifying critical heel and toe stress points. This study corroborates their findings, showing similar stress patterns under simulated loading conditions. The GRF results align with those reported by Ferris et al. [26] and Grabowski and D'Andrea [27], highlighting the importance of double-peaked GRF profiles in simulating natural gait mechanics. Mahmoodi et al. [12] explored prosthetic designs that consider specific GRF and rollover shapes, offering valuable guidance in balancing weight, stiffness, and energy return. While Tryggvason et al. [13] emphasized material properties such as aluminum alloys, the integration of optimization techniques in this study extends the scope of material performance enhancement. Tabucol et al. [16] utilized FEA combined with optimization for stiffness properties, and this research expands upon their methodology by incorporating LHS and Kriging surrogate modeling, enhancing the efficiency of design variable exploration.

Although this study aligns with prior research, it has limitations, such as the assumption of linear elastic material behavior in the FEA simulations. This assumption may not fully capture the non-linear dynamics inherent in prosthetic designs. Furthermore, although effective, the focus on 6061-T6 aluminum alloy may not account for the potential benefits of alternative materials, such as carbon fiber composites, which could offer improved strength-to-weight ratios.

Additionally, the reliance on standard loading conditions limits the generalizability of the findings to a diverse range of user profiles, particularly those with varying activity levels and body weights.

Despite presenting a comprehensive optimization framework combining Latin Hypercube Sampling (LHS), Kriging surrogate modeling, and Multi-Objective Genetic Algorithm (MOGA) for designing aluminum-based ESR prosthetic feet, the study has several limitations. One limitation is the absence of experimental validation owing to prototype availability and budget constraints. As such, the findings rely solely on finite element simulations, and future studies incorporating physical testing would provide further confidence in the model predictions and structural performance.

Another limitation is that the FEA in this study uses a 2D static model with linear elastic assumptions, which simplifies computational requirements but may overlook complex three-dimensional and nonlinear behaviors observed in real-world prosthetic foot usage. Finally, while the study focuses on aluminum alloy for its cost-effectiveness, comparing it with alternative materials like carbon fiber or titanium could enhance the generalizability and applicability of the proposed framework.

Future research could incorporate alternative materials and non-linear properties in FEA simulations to address these limitations, thereby enhancing prosthetic performance. Additionally, long-term studies involving diverse user profiles, including body weight, gait analysis, and activity levels, would provide valuable insights for optimizing prosthetic foot designs. Moreover, developing optimization methods tailored to individual biomechanical needs could improve the personalization and functionality of prosthetic devices, advancing the field further.

7. Conclusion

This study developed an optimized design for Energy Storage and Return (ESR) prosthetic feet, focusing on reducing weight and enhancing stiffness to improve biomechanical performance and user comfort. Advanced optimization techniques, including Latin Hypercube Sampling (LHS), Kriging, and Multi-Objective Genetic Algorithm (MOGA), effectively balanced energy return, load-bearing capacity, and biomechanical adaptability. The sensitivity analysis identified middle and lower blade thicknesses as key factors in regulating structural performance, ensuring efficient force distribution, and minimizing stress concentrations, particularly at the heel. The lightweight yet durable Aluminum Alloy 6061-T6 selection was optimal for a strength-to-weight ratio, enabling efficient load bearing while minimizing material strain. These findings demonstrate that combining advanced optimization methods with material selection improves the ESR prosthetic structural strength, weight, and energy efficiency, ultimately reducing the risk of overuse injuries. Future research could explore alternative materials, such as titanium alloys or composites, which may offer enhanced strength-to-weight ratios and further optimization strategies tailored to diverse user profiles and activity levels.

Author Contributions: S.R. developed Conceptualization, Formal Analysis, Investigation, Writing—Review and Editing, Visualization, and Supervision. A.S. developed Investigation, Methodology, Resources, Software, Validation, and Writing - Original draft. All authors discussed the results and contributed to the final manuscript.

Funding: The authors declare that no funds, grants, or other support were received during the preparation of this manuscript.

Conflict of Interest: All authors declare that there is no conflict of interest.

References

[1] Hafner, B.J., Sanders, J.E., Czerniecki, J.M., Fergason, J., Transtibial energy-storage-and-return prosthetic devices: a review of energy concepts and a proposed nomenclature, J. Rehabil. Res. Dev., 39(1) (2002) 1-11.

[2] Waters, R.L., Mulroy, S., The energy expenditure of normal and pathologic gait, Gait & Posture, 9(3) (1999) 207-231.

[3] Klodd, E., Hansen, A., Fatone, S., Edwards, M., Effects of prosthetic foot forefoot flexibility on gait of unilateral transtibial prosthesis users, J. Rehabil. Res. Dev., 47(9) (2010) 899-910.

[4] Fey, N. P., Klute, G. K., and Neptune, R. R., Optimization of Prosthetic Foot Stiffness to Reduce Metabolic Cost and Intact Knee Loading During Below-Knee Amputee Walking: A Theoretical Study, ASME J Biomech Eng., 134(11) (2012) 111005.

[5] Hafner, B.J., Sanders, J.E., Czerniecki, J., Fergason, J., Energy storage and return prostheses: does patient perception correlate with biomechanical analysis?, Clin. Biomech. (Bristol), 17(5) (2002) 325-344.

[6] Huang, T.W., Shorter, K.A., Adamczyk, P.G., Kuo, A.D., Mechanical and energetic consequences of reduced ankle plantar-flexion in human walking, J. Exp. Biol., 218(Pt 22) (2015) 3541-3550.

[7] Fey, N.P., Klute, G.K., Neptune, R.R., The influence of energy storage and return foot stiffness on walking mechanics and muscle activity in below-knee amputees, Clin. Biomech. (Bristol), 26(10) (2011) 1025-1032.

[8] Mohanad, F., Hasan, S., Emad, S., Optimal material selection for manufacturing prosthetic foot, Pertanika J. Sci. Technol., 30 (2022)

[9] Mangera, T., Kienhöfer, F., Carlson, K.J., Conning, M., Brown, A., Govender, G., Optimal material selection for the construction of a paediatric prosthetic knee, Proc. Inst. Mech. Eng. L J. Mater. Des. Appl., 232 (2018) 137-147.

[10] Bonnet, X., Pillet, H., Fodé, P., Lavaste, F., Skalli, W., Finite element modelling of an energy-storing prosthetic foot during the stance phase of transtibial amputee gait, Proc. Inst. Mech. Eng. H J. Eng. Med., 226 (2012) 70-75.

[11] Omasta, M., Paloušek, D., Návrat, T., Rosický, J., Finite element analysis for the evaluation of the structural behaviour of a prosthesis for trans-tibial amputees, Med. Eng. Phys., 34 (2012) 38-45.

[12] Mahmoodi, P., Aristodemou, S., Ransing, R., Owen, N., Friswell, M., Prosthetic foot design optimisation based on roll-over shape and ground reaction force characteristics, Proc. Inst. Mech. Eng. C J. Mech. Eng. Sci., 231(17) (2017) 3093-3103.

[13] Tryggvason, H., Starker, F., Lecomte, C., and Jonsdottir, F., Modeling and simulation in the design process of a prosthetic foot, Proc. Eur. Conf. Comput. Mech., (2017) 398-405.

[14] Kumar, K., and Sai, S., Finite element analysis on prosthetic leg under different loads and flexion angles for medical applications, J. Mech. Energy Eng., 6(2) (2022).

[15] Tryggvason, H., Starker, F., Lecomte, C., and Jonsdottir, F., Use of Dynamic FEA for Design Modification and Energy Analysis of a Variable Stiffness Prosthetic Foot, Appl. Sci., 10(2) (2020) 650.

[16] Tabucol, J., Brugo, T.M., Povolo, M., Leopaldi, M., Oddsson, M., Carloni, R., and Zucchelli, A., Structural FEA-Based Design and Functionality Verification Methodology of Energy-Storing-and-Releasing Prosthetic Feet, Appl. Sci., 12(1) (2022) 97.

[17] Kumar, S., Sujatha, C., & Srinivasan, S. (2023). Optimal design of magnetorheological valve using the coupling of FE magnetic analysis and MOGA optimization for prosthetic ankle. Journal of Vibration Engineering & Technologies, 12, 10.1007/s42417-023-00974-w.

[18] Kumar, S., Chandramohan, S., & Sujatha, S. (2024). Geometric optimization of magnetorheological damper for prosthetic ankles using artificial neural networks. Mechatronics, 98, 103108.

[19] Li, M., Li, G., and Azarm, S., A Kriging Metamodel Assisted Multi-Objective Genetic Algorithm for Design Optimization, J. Mech. Des., 130(3) (2008) 031401.

[20] Liu, C., Souza De Cursi, E., El Hami, A., and Eid, M., Application of Latin Hypercube Sampling Based Kriging Surrogate Models in Reliability Assessment, Science J. Appl. Math. Stat., 3(6) (2015) 263-274.

[21] Masum, H., Bhaumik, S., and Ray, R., Conceptual Design of a Powered Ankle-Foot Prosthesis for Walking with Inversion and Eversion, Procedia Technol., 14 (2014) 228-235.

[22] Mitchell, M., Craig, K., Kyberd, P., Biden, E., and Bush, G., Design and Development of Ankle-Foot Prosthesis with Delayed Release of Plantarflexion, J. Rehabil. Res. Dev., 50(3) (2013) 409-422.

[23] Bateni, H., & Olney, S.J., Effect of the weight of prosthetic components on the gait of transtibial amputees, JPO Journal of Prosthetics and Orthotics, 16 (2004) 113-120.

[24] Rao, Y., Yang, N., Gao, T., Zhang, S., Shi, H., Lu, Y., Ren, S., and Huang, H., Effects of peak ankle dorsiflexion angle on lower extremity biomechanics and pelvic motion during walking and jogging, Front. Neurol., 14 (2024) 1269061.

[25] Clites, T., Shepherd, M., Ingraham, K., Wontorcik, L., and Rouse, E., Understanding Patient Preference in Prosthetic Ankle Stiffness, J. NeuroEngineering Rehabil., 18 (2021).

[26] Grabowski, A. M., and D'Andrea, S., Effects of a powered ankle-foot prosthesis on kinetic loading of the unaffected leg during level-ground walking, J. Neuroeng. Rehabil., 10 (2013).

[27] Ferris, A. E., Aldridge, J. M., Rábago, C. A., and Wilken, J. M., Evaluation of a powered ankle-foot prosthetic system during walking, Arch. Phys. Med. Rehabil., 93(11) (2012) 1911-1918.

[28] Jones, D. R., Schonlau, M., and Welch, W. J., Efficient Global Optimization of Expensive Black-Box Functions, J. Glob. Optim., 13, 455–492 (1998).

[29] Matheron, G., Principles of Geostatistics, Econ. Geol., 58, 1246–1266 (1963).

[30] Holland, J. H., Genetic Algorithms, Sci. Am., 267(3), 66–73 (1992).

[31] Ariyarit, A., Rooppakhun, S., Puangchaum, W., and Phiboon, T., Design Optimization of Alloy Wheels Based on a Dynamic Cornering Fatigue Test Using Finite Element Analysis and Multi-Additional Sampling of Efficient Global Optimization, Symmetry, 15, 2169 (2023).

[32] Horn, J., Nafpliotis, N., and Goldberg, D. E., A Niched Pareto Genetic Algorithm for Multiobjective Optimization, Proc. 1st IEEE Conf. Evol. Comput., 1, 82–87 (1994).

[33] Borisut, P., and Nuchitprasittichai, A., Adaptive Latin Hypercube Sampling for a Surrogate-Based Optimization with Artificial Neural Network, Processes, 11, 3232 (2023).

[34] International Organization for Standardization, ISO 10328: 2006 - Prosthetics – Structural Testing of Lower-Limb Prostheses, ISO, 2006.

[35] ASM International, Metals Handbook, Vol. 2 - Properties and Selection: Nonferrous Alloys and Special-Purpose Materials, 10th ed., ASM International, 1990.

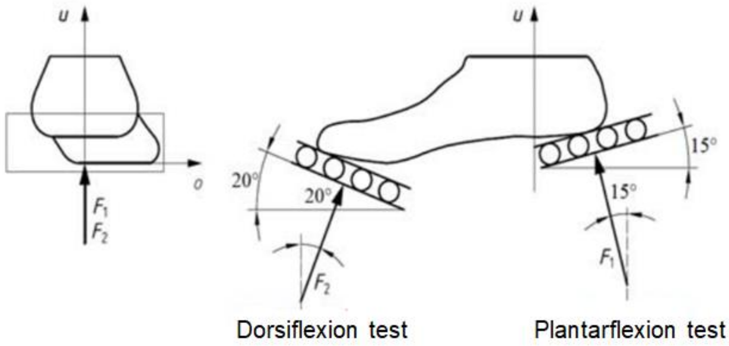

Figure 1. Loading conditions and recommended angles for prosthetic foot testing according to ISO 10328 standards

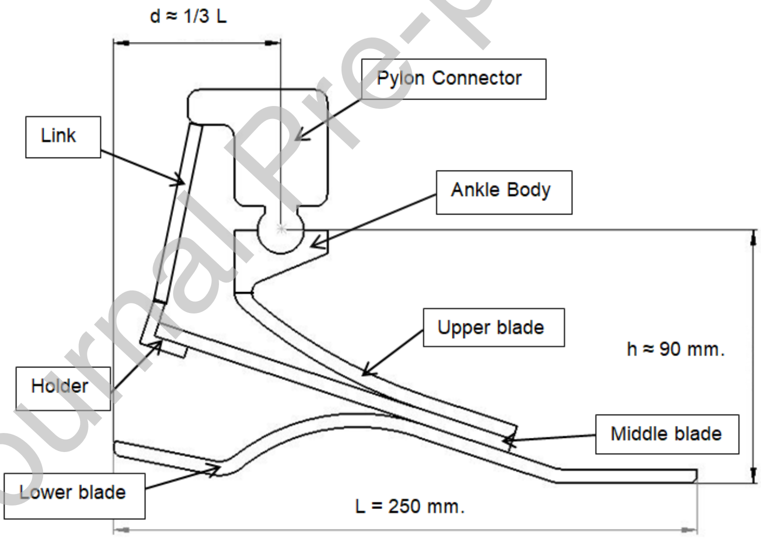

Figure 2. Functional groups and Dimensions

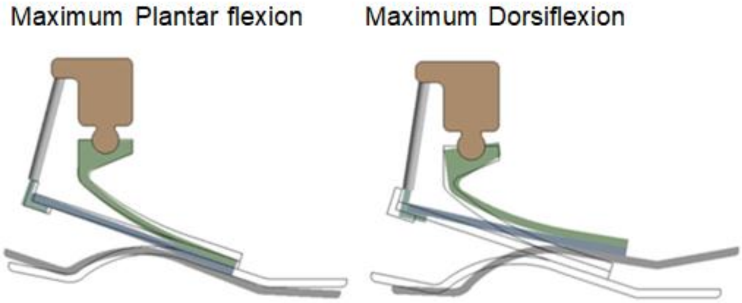

Figure 3. Deflection of the blades occurs when the foot prosthesis is loaded at the heel and the forefoot.

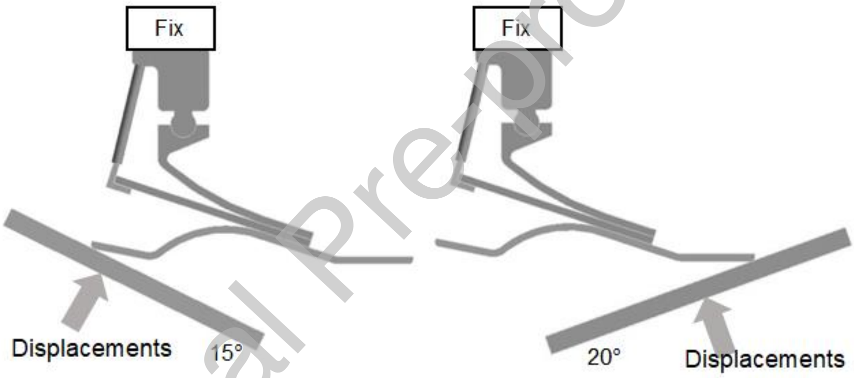

Figure 4. Schematic representation of the boundary conditions applied to the prosthetic foot model

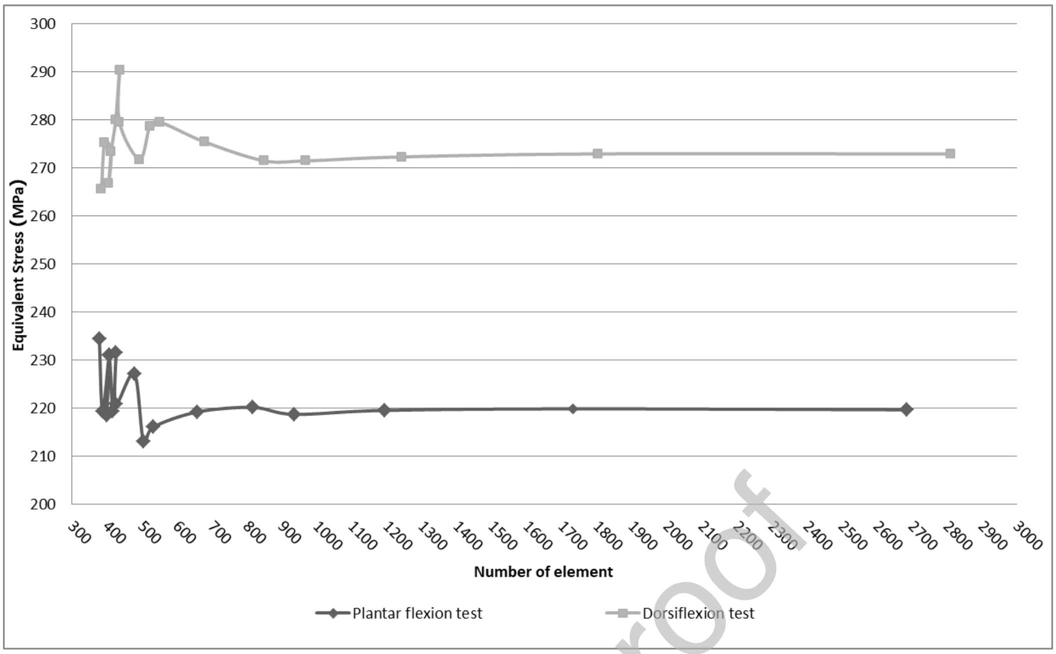

Figure 5. Convergence test of FE results

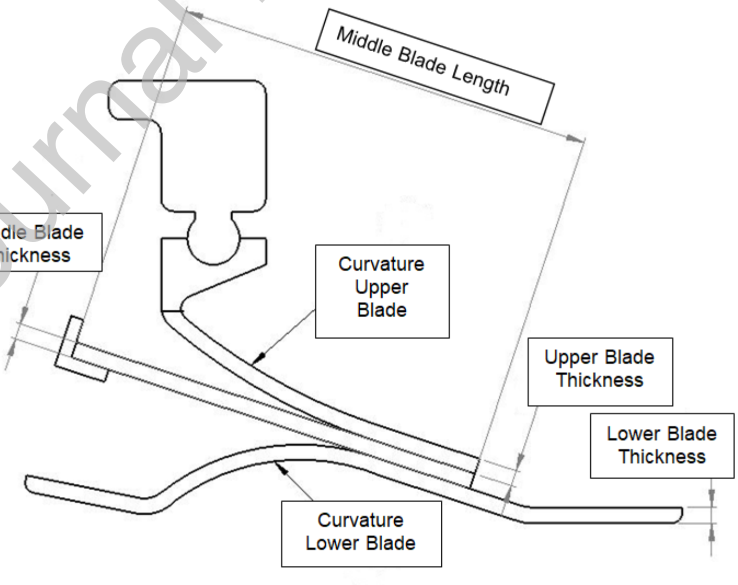

Figure 6. Design variables of prosthesis

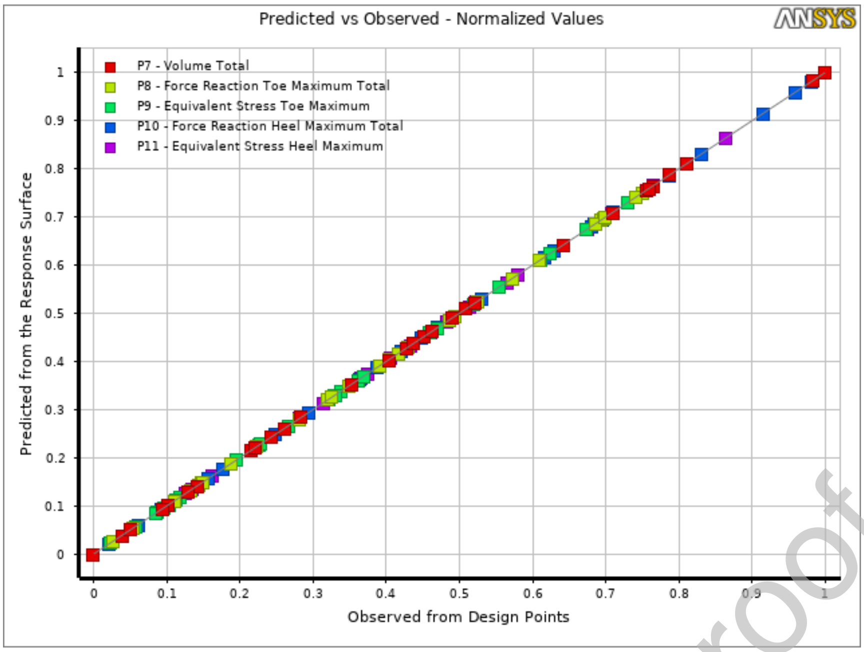

Figure 7. Model Validation: Predicted vs. Observed for Kriging Surrogate Model.

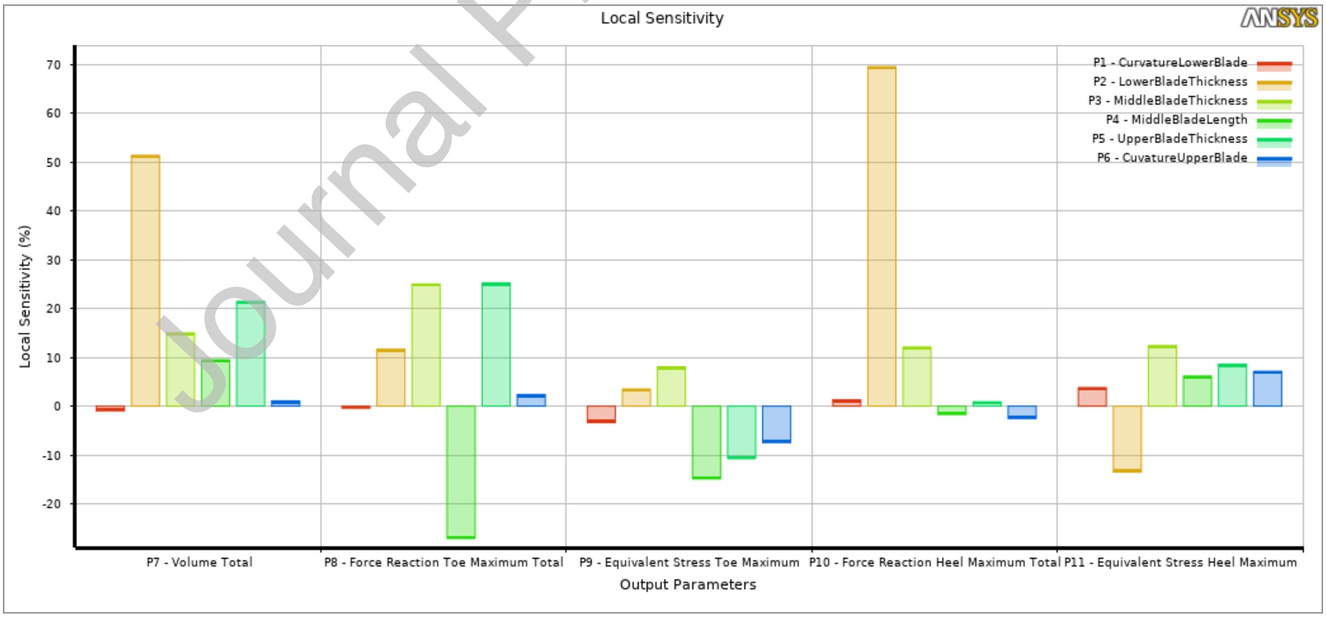

Figure 8. Sensitivity plot showing the influence of design variables on key output parameters

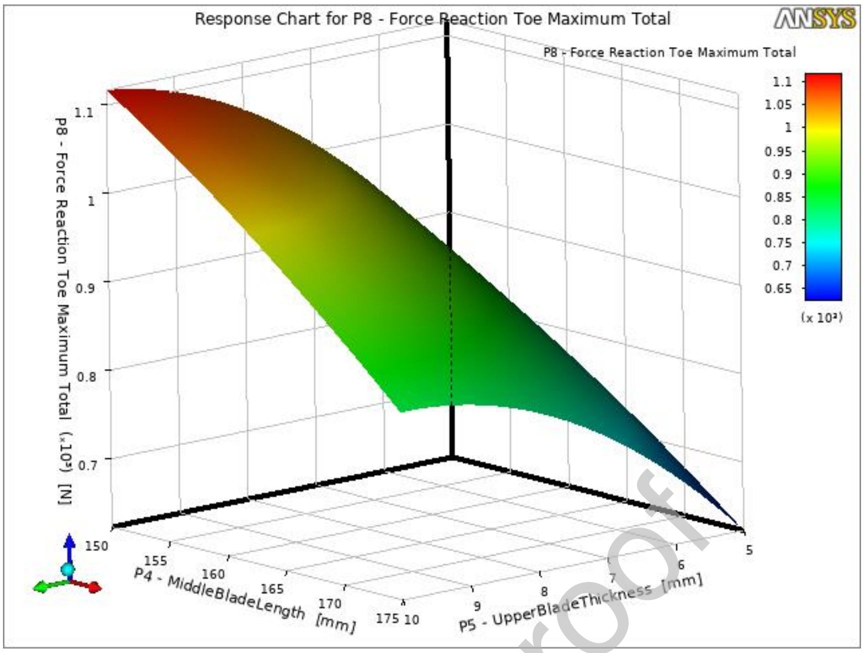

Figure 9. Response surface plot of the maximum force reaction at the toe

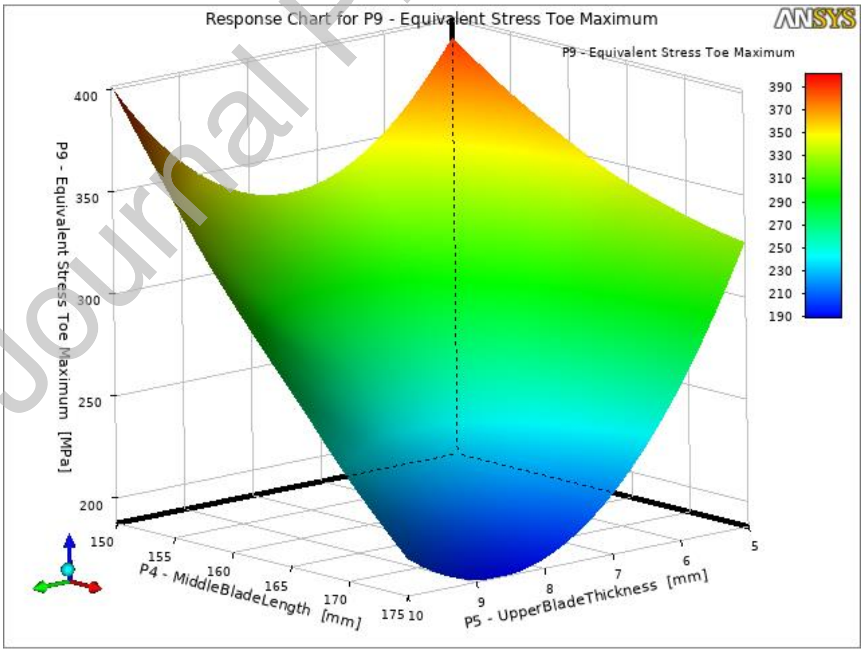

Figure 10. Response surface plot of the maximum equivalent stress at the toe

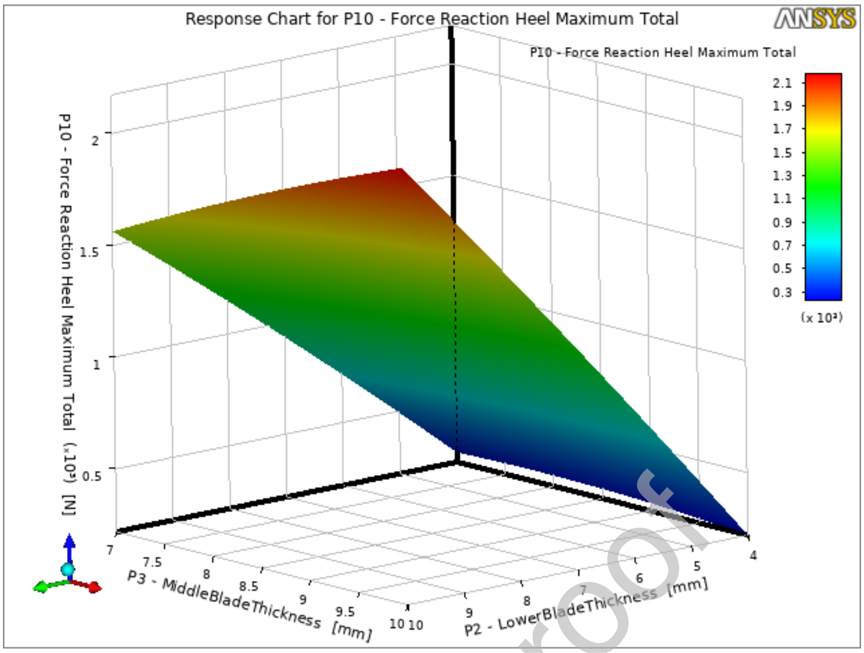

Figure 11. Response surface plot of the maximum force reaction at the heel

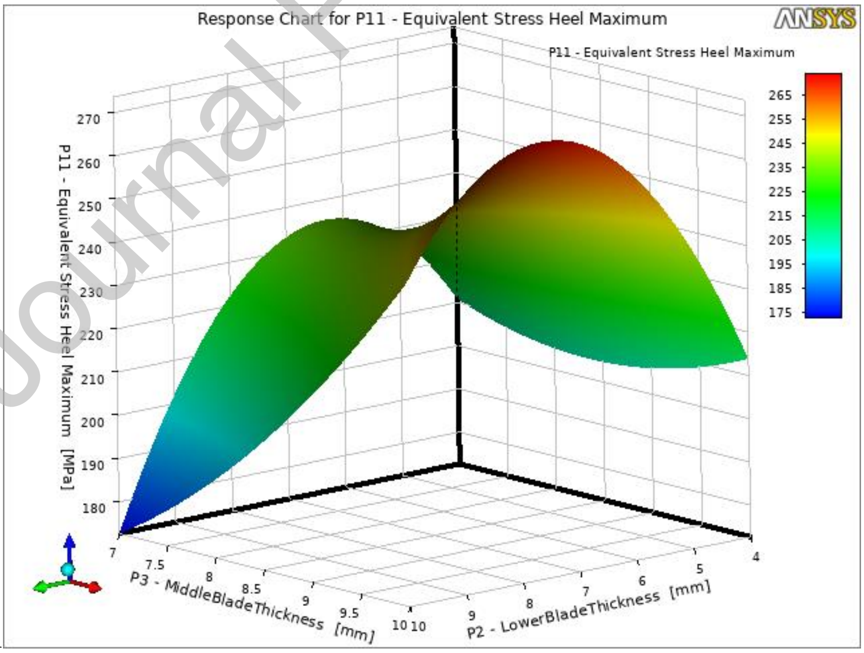

Figure 12. Response surface plot of the maximum equivalent stress at the heel

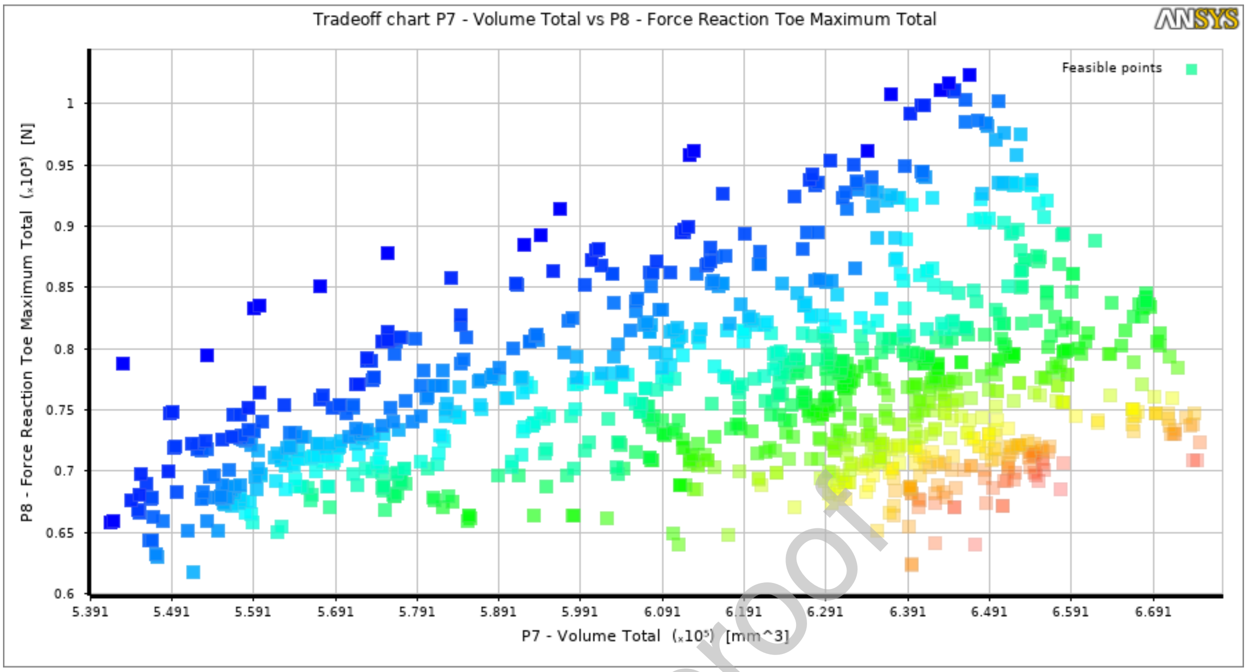

Figure 13. Tradeoff chart comparing total volume and maximum force reaction at the toe, highlighting the balance between material efficiency and force distribution for optimal prosthetic foot design.

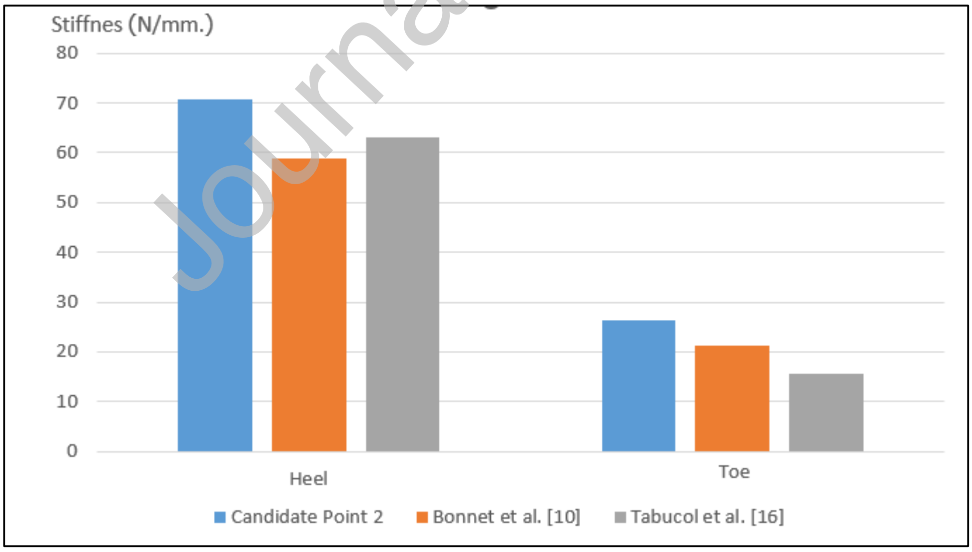

Figure 14. Comparison of the stiffness with reference studies.

Table 1: Design variables of prosthesis

	Parameter	Min value	Max value
P1	Upper blade thickness (mm.)	5	10
P2	Curvature upper blade (mm.)	190	220
P3	Middle blade thickness (mm.)	7	10
P4	Middle blade length (mm.)	150	175
P5	Lower blade thickness (mm.)	4	10
P6	Curvature lower blade (mm.)	60	10

Table 2: Mechanical Properties of Aluminum Alloy 6061-T6.

Property	Density (kg/m^3)	Yield Strength (MPa)	Ultimate Strength (MPa)	Elongation (%)	Modulus of Elasticity (GPa)
	2703	275	310	17	68.9

Table 3: Design Parameters of Candidate Points

Name	P1	P2	P3	P4	P5	P6
Candidate Point 1	65.64	5.27	7.04	172.72	6.28	191.44
Candidate Point 2	80.66	5.90	7.01	156.10	6.24	216.49
Candidate Point 3	69.14	5.67	7.16	170.43	5.81	190.48
Candidate Point 4	89.81	8.96	9.97	150.97	9.81	211.26
Candidate Point 5	77.76	4.02	7.07	151.58	5.03	193.74

Table 4: Performance Outputs of Candidate Points

Name	P7	P8	P9	P10	P11	Plantar flexion (°)	Dorsiflexion (°)
Candidate Point 1	541732.11	658.11	163.41	648.68	215.88	-6.63	10.19
Candidate Point 2	543138.77	788.89	219.65	707.59	215.58	-6.84	10.33
Candidate Point 3	545070.51	669.18	196.66	726.22	218.78	-6.67	9.95
Candidate Point 4	670220.50	1367.30	287.59	1901.70	290.19	-7.22	9.86
Candidate Point 5	488250.22	682.78	202.52	249.48	221.74	-6.63	12.54

Declaration of interests

☒The authors declare that they have no known competing financial interests or personal relationships that could have appeared to influence the work reported in this paper.

☐The authors declare the following financial interests/personal relationships which may be considered as potential competing interests: